



Combined Upper Limits on Standard Model Higgs Boson Production from the DØ Experiment in up to 6.7 fb^{-1} of data

The DØ Collaboration
URL <http://www-d0.fnal.gov>
(Dated: July 26, 2010)

Searches for standard model (SM) Higgs boson production in $p\bar{p}$ collisions at $\sqrt{s} = 1.96 \text{ TeV}$ are carried out for Higgs boson masses (M_H) in the range $100 \leq M_H \leq 200 \text{ GeV}$. The contributing production processes include associated production ($q\bar{q} \rightarrow VH$, $V = W/Z$), gluon-gluon fusion ($gg \rightarrow H$), and vector boson fusion ($q\bar{q} \rightarrow q'\bar{q}'H$). Analyses are conducted in 73 distinct channels with integrated luminosities ranging from 2.1 to 6.7 fb^{-1} . As no significant excess is observed, we set upper limits on standard model Higgs boson production. The observed 95% C.L. limits are a factor of 2.65 (1.03) higher than the predicted standard model cross section at $M_H = 115$ (165) GeV while the expected limits are a factor of 2.31 (1.14) higher than the standard model predicted cross section for the same masses.

I. INTRODUCTION

Despite its success as a predictive theory, the standard model (SM) of particle physics remains incomplete without an explanation of electroweak (EW) symmetry breaking. The simplest proposed mechanism involves the introduction of a complex doublet of scalar fields that generate the masses of the EW vector bosons. Besides accounting for electroweak bosons' longitudinal polarizations, this so-called Higgs mechanism also gives rise to a single scalar boson with an unknown mass. Direct searches in $e^+e^- \rightarrow Z^* \rightarrow ZH$ at the Large Electron Positron (LEP) collider yield a lower mass limit of $M_H > 114.4$ GeV [1] while precision electroweak data yield the indirect constraint $M_H < 157$ GeV [2], with both limits set at 95% confidence level (C.L.). When also considering the direct limit, the indirect constraint predicts $M_H < 186$ GeV, indicating that the range currently probed at the Fermilab Tevatron, $100 \leq M_H \leq 200$ GeV is the most important search region for a SM Higgs boson.

In this note, we combine the results of direct searches for SM Higgs bosons in $p\bar{p}$ collisions at $\sqrt{s} = 1.96$ TeV recorded by the DØ experiment [3]. The analyses combined here seek signals of Higgs bosons produced in association with vector bosons ($q\bar{q} \rightarrow VH$), through gluon-gluon fusion (GGF) ($gg \rightarrow H$), through vector boson fusion (VBF) ($q\bar{q} \rightarrow q'\bar{q}'H$), and in association with top quarks ($t\bar{t} \rightarrow t\bar{t}H$). The analyses utilize data corresponding to integrated luminosities ranging from 2.1 to 6.7 fb⁻¹, collected from 2002 to 2010. The dominant Higgs boson decay modes studied are $H \rightarrow b\bar{b}$, $H \rightarrow W^+W^-$, $H \rightarrow \tau^+\tau^-$ and $H \rightarrow \gamma\gamma$, depending on the final state. The searches are organized into 73 analysis subsets comprising different production, decay and final state particle configurations, each designed to isolate a particular Higgs boson production and decay mode. In order to facilitate proper combination of signals, the analyses were designed to be mutually exclusive after analysis selections. Searches for several final states are performed in two distinct epochs of data collection: before and after the 2006 DØ detector upgrade. The largest changes made during the upgrade were the addition of a new layer to the silicon detector nearest to the beam-line and an upgrade of the trigger system. The two epochs are denoted as Run IIa (1.1 fb⁻¹) and Run IIb (on-going, with up to 5.6 fb⁻¹ analyzed in this note).

The analyses used in this combination [4–14] are outlined in Table I. In the cases of $p\bar{p} \rightarrow VH$ production, we search for a Higgs boson decaying to two bottom quarks, two tau leptons, or two W^\pm bosons (the latter case is discussed below). The decays of the vector bosons further define the analyzed final states. To isolate $H \rightarrow b\bar{b}$ decays, an algorithm for identifying jets consistent with the decay of a heavy-flavor quark is applied to each jet (b -tagging). Several kinematic variables sensitive to displaced jet vertices and jet tracks with large transverse impact parameters relative to the hard-scatter vertices are combined using a multivariate analysis technique. The final output variable produced from the algorithm distinguishes heavy-flavor quark decays from jets arising from light-flavor quarks or gluons. Over time, the algorithm has improved, so some analyses use an older algorithm based on a neural-network (NN) while others use a newer algorithm based on a decision tree (DTree) [15]. In either case, by adjusting a minimum requirement on the b -tagging output a spectrum of increasingly stringent b -tagging operating points is achieved, each with a different signal efficiency and fake rate.

For the $WH \rightarrow \ell\nu b\bar{b}$, $ZH \rightarrow \nu\bar{\nu} b\bar{b}$ and $ZH \rightarrow \ell\bar{\ell} b\bar{b}$ processes ($\ell = e, \mu$), the analyses are separated into two groups: one in which two of the jets were b -tagged with a loose tag requirement ($WH \rightarrow \ell\nu b\bar{b}$) or one loose and one tight tag requirement ($ZH \rightarrow \nu\bar{\nu} b\bar{b}$ and $ZH \rightarrow \ell\bar{\ell} b\bar{b}$) (double b -tag or DT) and one group in which only one jet was tagged with a tight tag requirement (single b -tag or ST). The ST selection excludes any additional loose tagged jets, rendering the ST and DT selections orthogonal. The ST selection results in a typical per-jet efficiency and fake rate of about 50% and 0.5%, while the DT selection yields 60% and 1.5%, respectively. For these analyses, each lepton flavor of the V boson decay ($\ell = e, \mu$) is treated as an independent channel. The $ZH \rightarrow \nu\bar{\nu} b\bar{b}$ analysis includes the signal contribution from $WH \rightarrow \ell\nu b\bar{b}$ production where the primary lepton from the W boson decay falls outside of the detector fiducial volume or is not identified as a lepton. Similarly, the $WH \rightarrow \ell\nu b\bar{b}$ analysis includes signal contributions from the $ZH \rightarrow \ell\bar{\ell} b\bar{b}$ analysis. The $X+H \rightarrow \tau\tau b\bar{b}/q\bar{q}\tau\tau$ analysis selects the $\tau\tau$ plus dijet final state with one τ decaying to μ and the other decaying hadronically. This analysis is sensitive to $ZH \rightarrow \tau\tau b\bar{b}$, $VH \rightarrow q\bar{q}\tau\tau$, GGF and VBF. The $t\bar{t}H \rightarrow t\bar{t}b\bar{b}$ search channel analyses final states with up to 3 b -tags where in addition to the $H \rightarrow b\bar{b}$ decay b -jets emerge due to top quark decays.

We also consider Higgs decays to two W^\pm bosons. For $VH \rightarrow VW^+W^-$ production, we search for leptonic V boson decays with three final states of same-signed leptons: $VWW \rightarrow e^\pm e^\pm + X$, $e^\pm \mu^\pm + X$, and $\mu^\pm \mu^\pm + X$. In the case of $H \rightarrow W^+W^-$ and $q\bar{q}H \rightarrow q\bar{q}W^+W^-$ production via vector boson fusion, we search for leptonic W boson decays with three final states of opposite-signed leptons: $WW \rightarrow e^+ \nu e^- \nu$, $e^\pm \nu \mu^\mp \nu$, and $\mu^+ \nu \mu^- \nu$. The $H \rightarrow e^\pm \nu \mu^\mp \nu$ analysis further separates events in three final states with 0 jets, 1 jet, and two or more jets. In addition we also consider final states originating from Higgs boson production in association with a vector boson (WH or ZH), where leptons may originate from the vector boson or Higgs boson decay. For the gluon fusion and vector boson fusion processes, $H \rightarrow b\bar{b}$ decays are not considered due to the large multijet background. A separate analysis considers the $H \rightarrow W^+W^- \rightarrow \ell\nu q\bar{q}$ decay chain. In all $H \rightarrow W^+W^-$ decays with $M_H < 2M_W$, at least one of the W bosons will be off mass shell. Additionally there can be a small contribution from $H \rightarrow ZZ$ decays, mostly in the $H \rightarrow W^+W^- \rightarrow ee/\mu\mu\nu\nu$

searches. In all cases, lepton selections include both electrons and muons ($\ell = e, \mu$), while τ leptons are included in the simulation and the selections necessarily have acceptance for secondary leptons from $\tau \rightarrow e/\mu$ decays. Finally, we include an analysis that searches for Higgs bosons decaying to two photons and produced via gluon-gluon fusion, vector boson fusion, and associated production mechanisms.

Since the most recent $D\bar{O}$ SM combined Higgs boson search results [16], we have updated the $WH \rightarrow \ell\nu b\bar{b}$, $ZH \rightarrow \nu\bar{\nu} b\bar{b}$, $ZH \rightarrow \ell\bar{\ell} b\bar{b}$, $VH \rightarrow VW^+W^-$, and $H \rightarrow W^+W^- \rightarrow e\nu\mu\nu$ analyses. The $H \rightarrow W^+W^- \rightarrow \ell\nu q\bar{q}$ channel is a new addition to the combination.

TABLE I: List of analysis channels, their corresponding integrated luminosities, and final discriminant variables used for setting limits (See Sect. I for details.) The final variables are in most cases decision-tree-based (DTree) or neural-network-based (NN) discriminants. In cases where not every sub-channel uses the same dataset, a range of integrated luminosities is given.

Channel	Luminosity (fb^{-1})	Final Variable	# Sub-Channels	Reference
$WH \rightarrow \ell\nu b\bar{b}$, ST/DT, 2/3 jet	5.3	DTree discriminant	16	[4]
$ZH \rightarrow \nu\bar{\nu} b\bar{b}$, ST/DT	5.2-6.4	DTree discriminant	4	[5]
$ZH \rightarrow \ell\bar{\ell} b\bar{b}$, ST/DT	4.2-6.2	DTree discriminant	20	[6]
$X+H \rightarrow \tau\tau b\bar{b}/q\bar{q}\tau\tau$	4.9	NN/DTree discriminant	2	[7, 8]
$H \rightarrow W^+W^- \rightarrow e\nu\mu\nu$, 0/1/2+ jet	6.7	DTree discriminant	6	[9]
$H \rightarrow W^+W^- \rightarrow ee/\mu\mu\nu\nu$	5.4	NN discriminant	2	[10]
$H \rightarrow W^+W^- \rightarrow \ell\nu q\bar{q}$	5.4	DTree discriminant	4	[11]
$VH \rightarrow VW^+W^-$	5.3	DTree discriminant	6	[12]
$H \rightarrow \gamma\gamma$	4.2	Di-photon Mass	1	[13]
$t\bar{t}H \rightarrow t\bar{t}b\bar{b}$	2.1	Scaled H_T	12	[14]

Most Higgs boson signals are simulated using PYTHIA [17], and CTEQ5L or CTEQ6L [18] leading-order (LO) parton distribution functions, but normalized to higher-order calculations. The $gg \rightarrow H$ production cross section is from Grazzini and de Florian [19], which is consistent with Ref. [20]. The PDFs used in these calculations are the Next-to-next-to Leading Order (NNLO) MSTW2008 set [21]. WH and ZH cross sections are from Baglio and Djouadi [22, 23], and did not change compared to values in [16]. These calculations include a thorough treatment of higher-order radiative corrections, particularly those involving b -quark loops. VBF cross sections are calculated at next-to-leading order (NLO) in QCD [27]. $t\bar{t}H$ signals are simulated with COMPHEP [28], and cross sections are calculated at NLO. The decay branching fractions are from HDECAY version 3.53 [25]. The Higgs production cross-sections and branching ratios used are listed in Table II.

The backgrounds from multijet production are obtained from data. Other backgrounds were generated with PYTHIA, ALPGEN [26], and COMPHEP [28], with PYTHIA providing parton-showering and hadronization for all generators. Background cross sections are normalized either to next-to-leading order (NLO) calculations from MCFM [24] or, when possible, to data control samples.

II. LIMIT CALCULATIONS

We combine results using the CL_s method with a negative log-likelihood ratio (LLR) test statistic [29]. The value of CL_s is defined as $CL_s = CL_{s+b}/CL_b$ where CL_{s+b} and CL_b are the confidence levels for the signal-plus-background hypothesis and the background-only hypothesis, respectively. These confidence levels are evaluated by integrating corresponding LLR distributions populated by simulating outcomes via pseudo-experiments. The results are combined by summing LLR values over all bins and channels. This method provides a robust means of combining individual channels while maintaining individual channel sensitivities and incorporating systematic uncertainties. Systematics are treated as Gaussian uncertainties on the expected number of signal and background events, not as outcomes of the limit calculations. This approach ensures that the uncertainties and their correlations are propagated to the outcome with their proper weights. The CL_s approach in this combination utilizes binned final discriminant variable distributions rather than a single-bin (fully integrated) value for each contributing analysis. The exclusion criteria are determined by increasing the signal cross section until $CL_s = 1 - \alpha$, which defines a signal cross section excluded at 95% confidence level for $\alpha = 0.05$.

TABLE II: The (N)NLO production cross sections and decay branching fractions for the SM Higgs boson used in this combination [19–22, 24, 25].

m_H (GeV)	$\sigma_{gg \rightarrow H}$ (fb)	σ_{WH} (fb)	σ_{ZH} (fb)	σ_{VBF} (fb)	σ_{ttH} (fb)	$B(H \rightarrow bb)$ (%)	$B(H \rightarrow c\bar{c})$ (%)	$B(H \rightarrow \tau^+\tau^-)$ (%)	$B(H \rightarrow W^+W^-)$ (%)	$B(H \rightarrow ZZ)$ (%)	$B(H \rightarrow \gamma\gamma)$ (%)
100	1861	291.9	169.8	99.5	8.00	80.33	3.542	7.920	1.052	0.1071	0.1505
105	1618	248.4	145.9	93.3	7.07	78.57	3.463	7.821	2.307	0.2035	0.1689
110	1413	212.0	125.7	87.1	6.25	75.90	3.343	7.622	4.585	0.4160	0.1870
115	1240	181.9	108.9	79.07	5.51	71.95	3.169	7.288	8.268	0.8298	0.2029
120	1093	156.4	94.4	71.65	4.86	66.49	2.927	6.789	13.64	1.527	0.2148
125	967	135.1	82.3	67.37	4.28	59.48	2.617	6.120	20.78	2.549	0.2204
130	858	116.9	71.9	62.5	3.77	51.18	2.252	5.305	29.43	3.858	0.2182
135	764	101.5	63.0	57.65	3.32	42.15	1.854	4.400	39.10	5.319	0.2077
140	682	88.3	55.3	52.59	2.93	33.04	1.453	3.472	49.16	6.715	0.1897
145	611	77.0	48.7	49.15	2.59	24.45	1.075	2.585	59.15	7.771	0.1653
150	548	67.3	42.9	45.67	2.29	16.71	0.7345	1.778	68.91	8.143	0.1357
155	492	58.9	37.9	42.19	2.03	9.88	0.4341	1.057	78.92	7.297	0.09997
160	439	50.8	33.1	38.59	1.80	3.74	0.1646	0.403	90.48	4.185	0.05365
165	389	44.6	30.0	36.09	1.60	1.29	0.05667	0.140	95.91	2.216	0.02330
170	349	40.2	26.6	33.58	1.43	0.854	0.03753	0.093	96.39	2.351	0.01598
175	314	35.6	23.7	31.11	1.27	0.663	0.02910	0.073	95.81	3.204	0.01236
180	283	31.4	21.1	28.57	1.14	0.535	0.02349	0.059	93.25	5.937	0.01024
185	255	28.2	18.9	26.81	1.01	0.415	0.01823	0.046	84.50	14.86	0.008128
190	231	25.1	17.0	24.88	0.90	0.340	0.01490	0.038	78.70	20.77	0.006774
195	210	22.4	15.3	23	0.79	0.292	0.01281	0.033	75.88	23.66	0.005919
200	192	20.0	13.7	21.19	0.70	0.257	0.01128	0.029	74.26	25.33	0.005285

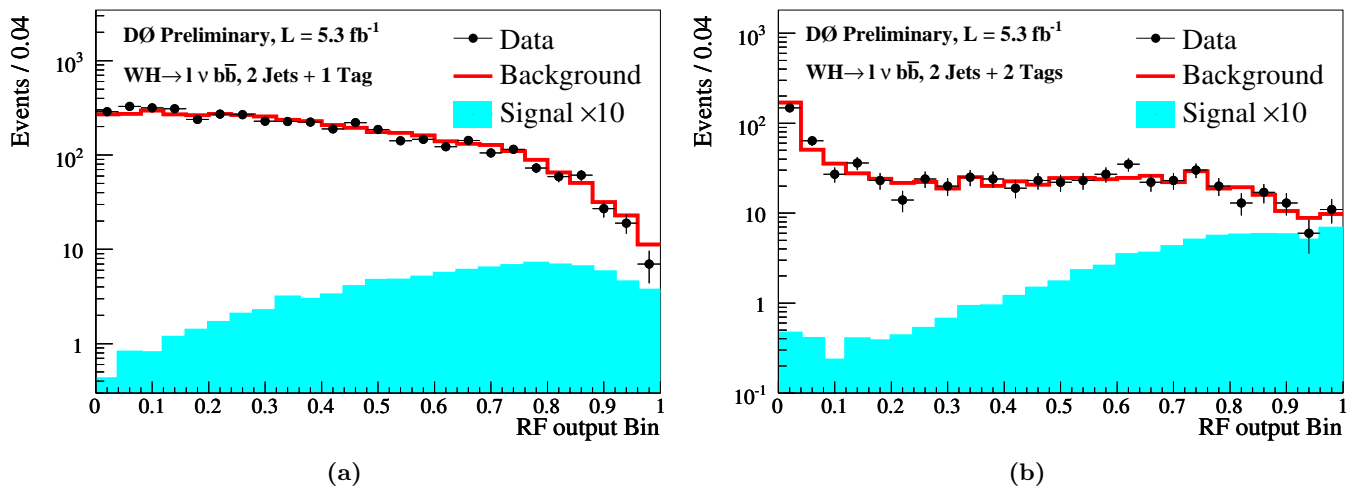


FIG. 1: Final variable distribution for the $WH \rightarrow \ell \nu b \bar{b}$ analysis in the 2-jet sub-channel for (a) ST, and (b) DT samples. The mass of the signal shown here is 115 GeV.

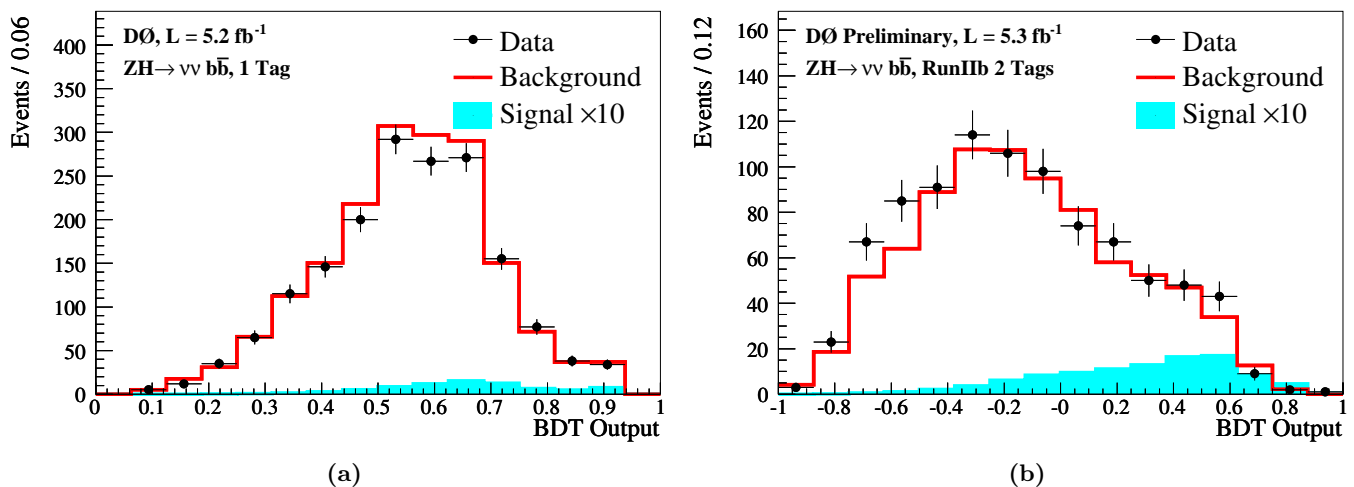


FIG. 2: Final variable distribution for the $ZH \rightarrow \nu \nu b \bar{b}$ analysis for (a) ST, and (b) DT samples. The mass of the signal shown here is 115 GeV.

A. Final Variable Preparation

The final variables for all analyses (See Table I) are shown in Figs. 1-9. In several of these figures, multiple contributing sub-channels are summed together. Most of the analyses are performed on a fine Higgs boson mass grid with 5 GeV steps. A 10 GeV grid was used in case of the $X+H \rightarrow \tau \tau b \bar{b} / q \bar{q} \tau \tau$ and $t \bar{t} H \rightarrow t \bar{t} b \bar{b}$ analyses.

B. Systematic Uncertainties

The systematic uncertainties differ between analyses for both the signals and backgrounds [4–14]. Here we summarize only the largest contributions. Most analyses carry an uncertainty on the integrated luminosity of 6.1% [30], while the overall normalization of other analyses is determined from the NNLO Z/γ^* cross section in data events near the peak of $Z \rightarrow \ell \ell$ decays. The $H \rightarrow b \bar{b}$ analyses have an uncertainty on the b -tagging rate of 1-9%. These analyses also have an uncertainty on the jet measurement and acceptances of $\sim 7\%$. All analyses include uncertainties associated with lepton measurement and acceptances, which range from 1-5% per lepton in the final state. The largest contribution for all analyses is the uncertainty on the background cross sections at 6-30% depending on the analysis channel and specific background. These values include both the uncertainties on the theoretical cross section calculations and

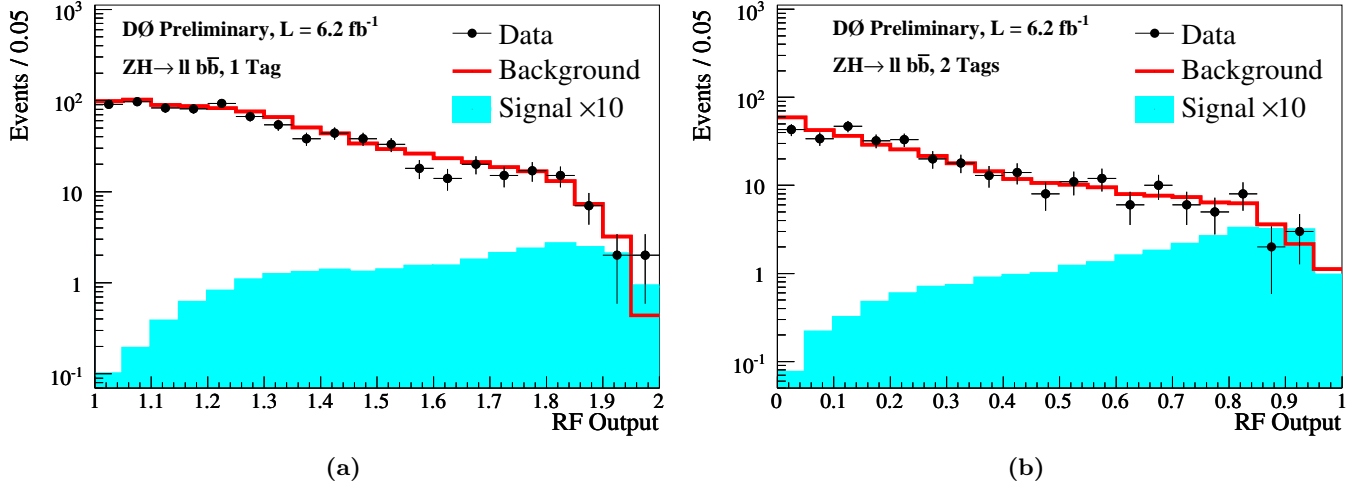


FIG. 3: Final variable distribution for the $ZH \rightarrow \ell\ell b\bar{b}$ analysis for (a) ST, and (b) DT samples, with all lepton channels combined. The mass of the signal shown here is 115 GeV.

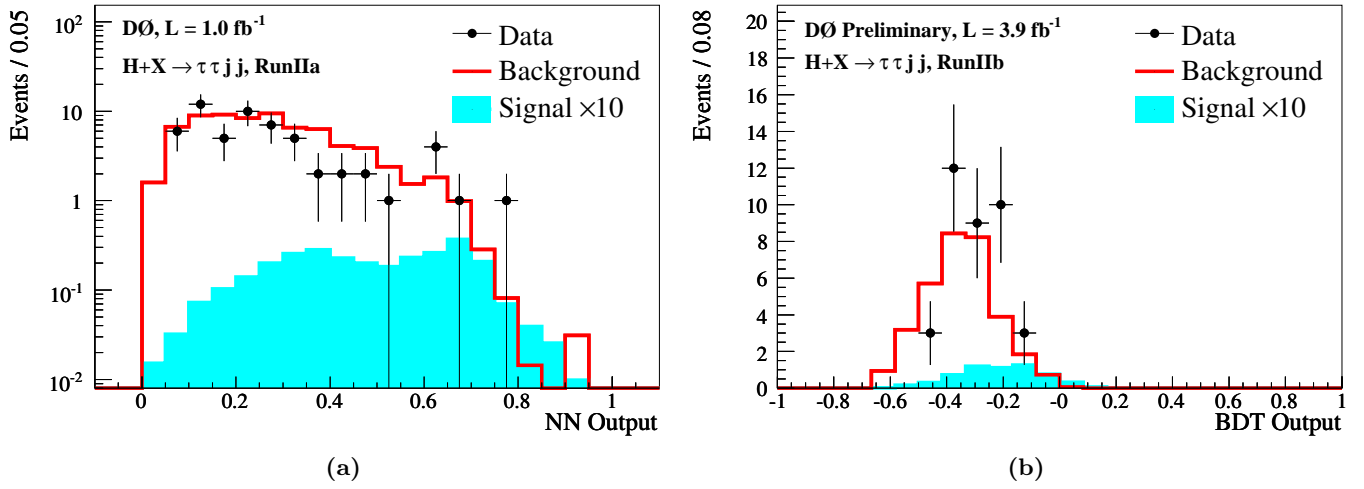


FIG. 4: Final variable distribution for the $X+H \rightarrow \tau\tau b\bar{b}/q\bar{q}\tau\tau$ analysis for (a) Run IIa, and (b) Run IIb. The mass of the signal shown here is 115 GeV.

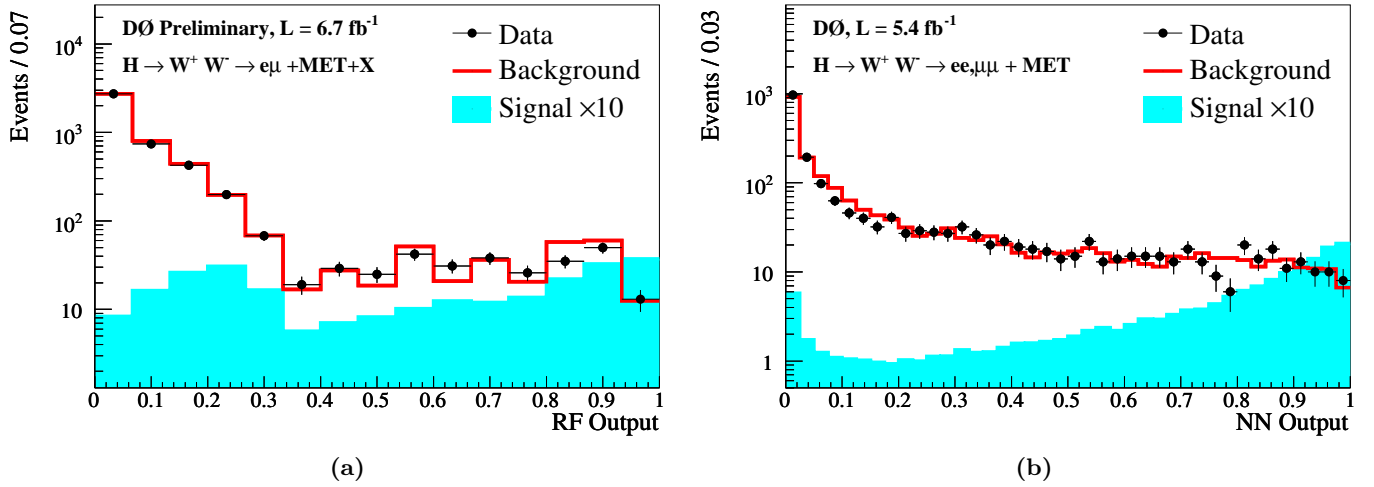


FIG. 5: Final variable distribution for the $H \rightarrow W^+W^- \rightarrow (ee, \mu\mu, e\mu)\nu\nu$ analysis, for the (a) $e\mu$, and (b) ee and $\mu\mu$ samples. The mass of the signal shown here is 165 GeV.

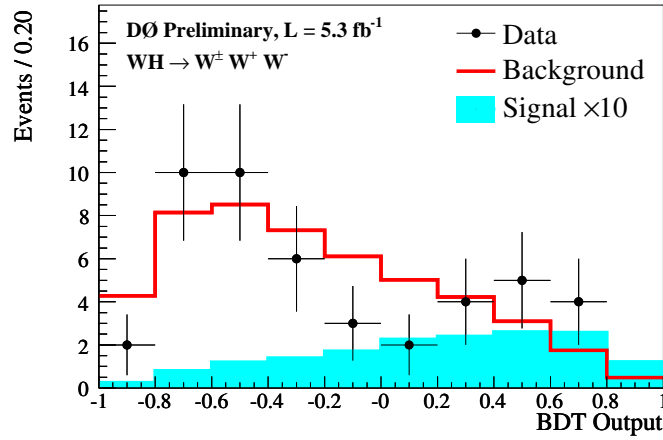


FIG. 6: Final variable distribution for the $VH \rightarrow VW^+W^-$ analysis with all lepton channels combined. The mass of the signal shown here is 165 GeV.

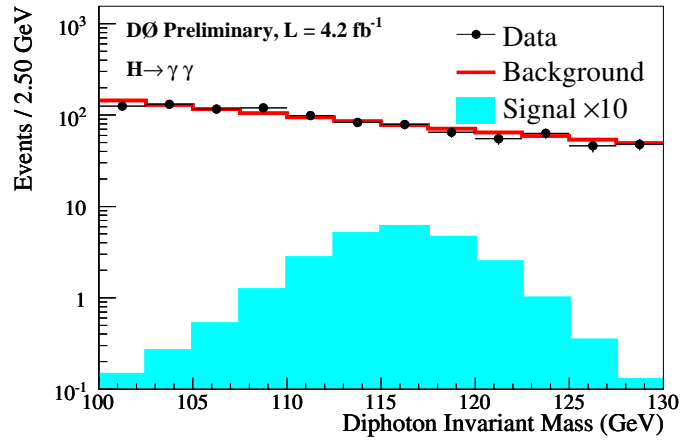


FIG. 7: Final variable distribution for the $H \rightarrow \gamma\gamma$ analysis. The mass of the signal shown here is 115 GeV.

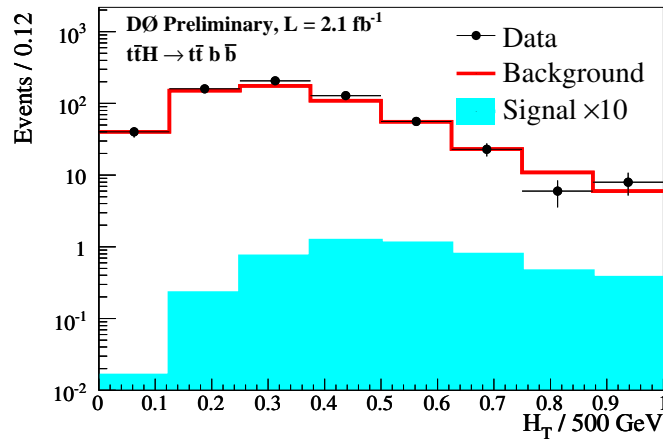


FIG. 8: Final variable distribution for the $t\bar{t}H \rightarrow t\bar{t}b\bar{b}$ analysis. The mass of the signal shown here is 115 GeV.

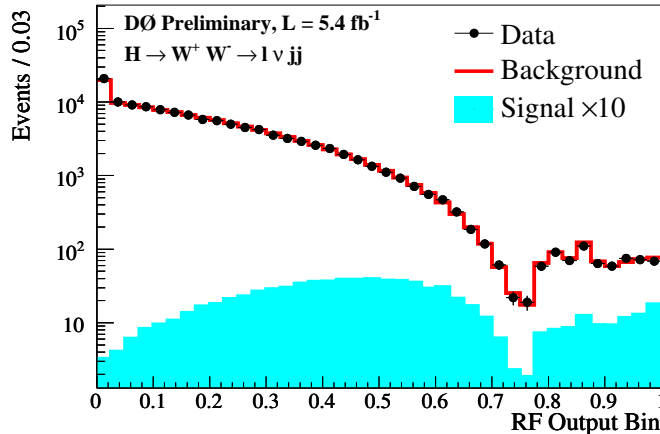


FIG. 9: Final variable distribution for the $H \rightarrow W^+ W^- \rightarrow \ell \nu q \bar{q}$ analysis with all lepton channels combined. The mass of the signal shown here is 165 GeV.

the uncertainties on the higher order correction (K) factors. The uncertainty on the expected multijet background is dominated by the statistics of the data sample from which it is estimated, and is considered separately from the other cross section uncertainties. The $H \rightarrow W^+ W^-$ and $H \rightarrow \gamma \gamma$ analyses also assign two 8% uncertainties to the NNLO GGF Higgs production cross section associated with the theoretical calculation and arising from uncertainty both in PDF and renormalization and hadronization scale. The $H \rightarrow W^+ W^- \rightarrow e \nu \mu \nu$ analysis applies a different uncertainty for each jet multiplicity final state, ranging from 6% to 80% [31]. In addition, several analyses incorporate shape-dependent uncertainties on the kinematics of the dominant backgrounds in the analyses. These shapes are derived from the potential deformations of the final variables due to generator and background modeling uncertainties. Further details on the systematic uncertainties are given in Table III.

The systematic uncertainties for background rates are generally several times larger than the signal expectation itself and are an important factor in the calculation of limits. Each systematic uncertainty is folded into the signal and background expectations in the limit calculation via Gaussian distributions. These Gaussian values are sampled for each Poisson MC trial (pseudo-experiment). Several of the systematic uncertainties, for example the jet energy scale uncertainty, also impact the shape of the final variable. These shape dependences were preserved in the description of systematic fluctuations for each Poisson trial. Correlations between systematic sources are carried through in the calculation. For example, the uncertainty on the integrated luminosity is held to be correlated between all signals and backgrounds and, thus, the same fluctuation in the luminosity is common to all channels for a single pseudo-experiment. All systematic uncertainties originating from a common source are held to be correlated, as detailed in Tables III and IV.

To minimize the degrading effects of systematics on the search sensitivity, the individual background contributions are fitted to the data observation by maximizing a likelihood function for each hypothesis [32]. The likelihood is a joint Poisson probability over the number of bins in the calculation and is a function of the nuisance parameters in the system and their associated uncertainties, which are given an additional Gaussian constraint associated with their prior predictions. The maximization of the likelihood function is performed over the nuisance parameters. A fit is performed to both the background-only (b) and signal-plus-background (s+b) hypothesis separately for each Poisson MC trial.

III. DERIVED UPPER LIMITS

We derive limits on SM Higgs boson production $\sigma \times B(H \rightarrow X)$ via the 73 individual analyses performed by DØ [4–14]. The limits are derived at 95% C.L. To facilitate model transparency and to accommodate analyses with different degrees of sensitivity, we present our results in terms of the ratio of 95% C.L. upper cross section limits to the SM predicted cross section as a function of Higgs boson mass. The SM prediction for Higgs boson production would therefore be considered excluded at 95% C.L. when this limit ratio falls below unity.

The individual analyses listed in Table I are grouped to evaluate combined limits over the range $100 \leq M_H \leq 200$ GeV. The $X+H \rightarrow \tau \tau b \bar{b} / q \bar{q} \tau \tau$ analysis contributes to the region $M_H \leq 145$ GeV, the $ZH \rightarrow \ell \ell b \bar{b}$ $ZH \rightarrow \nu \bar{\nu} b \bar{b}$ $WH \rightarrow \ell \nu b \bar{b}$ and $H \rightarrow \gamma \gamma$ analyses contribute for $M_H \leq 150$ GeV, the $VH \rightarrow VW^+ W^-$ analyses contribute for $M_H \geq$

TABLE III: List of leading correlated systematic uncertainties in % change of the total event yield, averaged over backgrounds and signals. All uncertainties within a group are considered 100% correlated across channels. The correlated systematic uncertainty on the background cross section (σ) and shape-dependent background modeling are subdivided according to the different background processes in each analysis. Uncertainties listed as shape only (s.o.) do not affect the total event yield but do affect the shape of the final variable.

Source	$WH \rightarrow e\nu b\bar{b}$	$WH \rightarrow \mu\nu b\bar{b}$	$VH \rightarrow VW^+W^- \rightarrow \ell\nu\ell\nu\ell\nu$
Luminosity	6.1	6.1	-
Normalization	-	-	6.1
Jet Energy Scale	2-5	2-5	-
Jet ID	1-2	1-2	-
Jet Triggers	-	-	2-5
Electron ID/Trigger	2-3	-	4-9
Muon ID/Trigger	-	3-5	2-4
b -Jet Tagging	9-11	9-11	-
Background cross section	6-20	6-20	6-7
Multijet	1.0	1.0	10-15
Shape-Dependent Bkgd Modeling	2-3	2-3	s.o.

Source	$ZH \rightarrow \nu\bar{\nu} b\bar{b}$	$ZH \rightarrow e^+e^- b\bar{b}$	$ZH \rightarrow \mu^+\mu^- b\bar{b}$
Luminosity	6.1	6.1	6.1
Jet Energy Scale	3.5	4.0	1.0
Jet ID	1.0	4.0	4.0
Jet Triggers	3.5	-	-
Electron ID/Trigger	0.4	-	-
Muon ID/Trigger	1-2	-	5.0
b -Jet Tagging	2-6	9.0	9.0
Background cross section	6-20	6-20	10-30
Multijet	25	20-60	20-50
Shape-Dependent Bkgd Modeling	s.o.	5.0	4.0

Source	$H \rightarrow W^+W^- \rightarrow \ell\nu\ell\nu$	$H \rightarrow W^+W^- \rightarrow \ell\nu jj$	$H \rightarrow \gamma\gamma$
Luminosity	6.1	6.1	6.1
Jet Energy Scale	4.0	1-2	-
Jet ID	1.0	0.3	-
Electron ID/Trigger	3-6	4.0	1.0
Muon ID/Trigger	4.0	4.0	-
Background cross section	6-10	6-20	6.0
Signal cross section	6-80	11	11
Multijet	2.0	3.0	1.0
Shape-Dependent Bkgd Modeling	2.0	s.o.	6.0

Source	$t\bar{t}H \rightarrow t\bar{t}b\bar{b}$	$X+H \rightarrow \tau\tau b\bar{b}/q\bar{q}\tau\tau$
Luminosity	6.1	6.1
Jet Energy Scale	-	4.5
Jet ID	-	2-3
Tau Energy Scale/ID	-	3.5
Electron ID/Trigger	2.5	-
Muon ID/Trigger	2	5-7
b -Jet Tagging	3-9	-
Background σ	10-20	6-20
Signal σ	-	11
Multijet	100	4-39

115 GeV, the $t\bar{t}H \rightarrow t\bar{t}b\bar{b}$ analysis contributes for $M_H \leq 155$ GeV, the $H \rightarrow W^+W^- \rightarrow (ee, \mu\mu, e\mu)\nu\nu$ analyses contribute for $M_H \geq 115$ GeV, and the $H \rightarrow W^+W^- \rightarrow \ell\nu jj$ analyses contribute for $M_H \geq 155$ GeV.

Figure 10 shows the expected and observed 95% C.L. cross section limit as a ratio to the SM cross section in the probed mass region ($100 \leq M_H \leq 200$ GeV), with all analyses combined. These results are also summarized in Table V. The LLR distributions for the full combination are shown in Fig. 11. Included in these figures are the median LLR values for the signal-plus-background hypothesis (LLR_{s+b}), background-only hypothesis (LLR_b), and the

TABLE IV: The correlation matrix for the analysis channels. All uncertainties within a group are considered 100% correlated across channels. The correlated systematic uncertainty on the background cross section (σ) is itself subdivided according to the different background processes in each analysis.

Source	$WH \rightarrow \ell\nu b\bar{b}$	$ZH \rightarrow \nu\bar{\nu} b\bar{b}$	$ZH \rightarrow \ell\bar{\ell} b\bar{b}$	$H \rightarrow W^+W^- \rightarrow \ell\nu\ell\nu$	$H \rightarrow W^+W^- \rightarrow \ell\nu jj$
Luminosity	×	×	×	×	×
Normalization					
Jet Energy Scale	×	×	×	×	×
Jet ID	×	×	×		×
Tau Energy Scale/ID					
Electron ID/Trigger	×	×	×	×	×
Muon ID/Trigger	×	×	×	×	×
b -Jet Tagging	×	×	×		
Background σ	×	×	×	×	×
Background Modeling					
Signal σ				×	×
Multijet					

Source	$VH \rightarrow VW^+W^-$	$H \rightarrow \gamma\gamma$	$X+H \rightarrow \tau\tau b\bar{b}/q\bar{q}\tau\tau$	$t\bar{t}H \rightarrow t\bar{t}b\bar{b}$
Luminosity		×	×	×
Normalization				
Jet Energy Scale			×	
Jet ID			×	
Tau Energy Scale/ID			×	
Electron ID/Trigger	×	×	×	×
Muon ID/Trigger	×		×	×
b -Jet Tagging				×
Background σ	×		×	×
Background Modeling				
Signal σ		×		
Multijet				

observed data (LLR_{obs}). The shaded bands represent the 1 and 2 standard deviation departures for LLR_b . Figure 12 shows the observed $1 - CL_S$ and its expected distributions for the background-only hypothesis as a function of the Higgs boson mass. These distributions can be interpreted as follows:

- The separation between LLR_b and LLR_{s+b} provides a measure of the discriminating power of the search. This is the ability of the analysis to separate the $s + b$ and b -only hypotheses.
- The width of the LLR_b distribution (shown here as one and two standard deviation provides an estimate of how sensitive the analysis is to a signal-like background fluctuation in the data, taking account of the presence of systematic uncertainties. For example, when a 1 standard deviation background fluctuation is large compared to the signal expectation, the analysis sensitivity is thereby limited.
- The value of LLR_{obs} relative to LLR_{s+b} and LLR_b indicates whether the data appear to be more like signal-plus-background or background-only. As noted above, the significance of any departures of LLR_{obs} from LLR_b can be evaluated by the width of the LLR_b distribution.
- The observed $1 - CL_S$ and its expected distributions can be directly interpreted as the level of exclusion of our search for each mass point.

IV. CONCLUSIONS

We present upper limits on standard model Higgs boson production derived from the 73 Higgs search analyses at $D\bar{O}$ including data corresponding to 2.1-6.7 fb^{-1} (See Table I). We combine these analyses and form new limits more sensitive than each individual limit. The observed (expected) 95% C.L. upper limit ratios to the SM Higgs boson production cross sections are 2.65 (2.31) at $M_H = 115$ GeV and 1.03 (1.14) at $M_H = 165$ GeV.

TABLE V: Combined 95% C.L. limits on $\sigma \times B(H \rightarrow X)$ for SM Higgs boson production. The limits are reported in units of the SM production cross section times branching fraction.

M_H (GeV)	100	105	110	115	120	125	130	135	140	145	150
Expected:	1.80	1.86	2.13	2.31	2.60	2.67	2.82	2.59	2.40	2.19	1.87
Observed:	1.40	1.69	1.44	2.65	3.50	4.16	3.16	4.17	3.53	3.29	2.43

M_H (GeV)	155	160	165	170	175	180	185	190	195	200
Expected:	1.62	1.21	1.14	1.36	1.60	1.92	2.40	2.93	3.40	3.96
Observed:	1.93	1.17	1.03	1.10	1.35	1.86	2.86	3.27	4.44	4.97

Acknowledgments

We thank the staffs at Fermilab and collaborating institutions, and acknowledge support from the DOE and NSF (USA); CEA and CNRS/IN2P3 (France); FASI, Rosatom and RFBR (Russia); CNPq, FAPERJ, FAPESP and FUNDUNESP (Brazil); DAE and DST (India); Colciencias (Colombia); CONACyT (Mexico); KRF and KOSEF (Korea); CONICET and UBACyT (Argentina); FOM (The Netherlands); STFC and the Royal Society (United Kingdom); MSMT and GACR (Czech Republic); CRC Program and NSERC (Canada); BMBF and DFG (Germany); SFI (Ireland); The Swedish Research Council (Sweden); and CAS and CNSF (China).

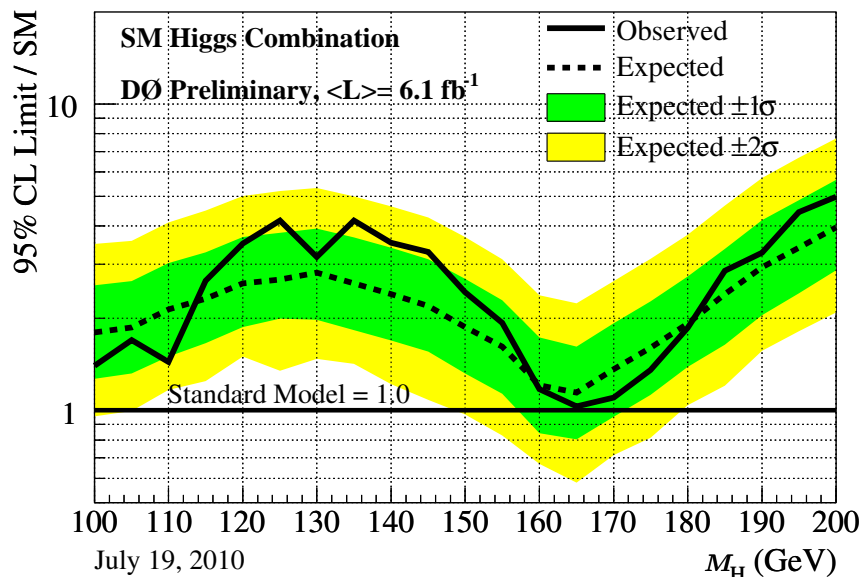


FIG. 10: Expected (median) and observed 95% C.L. cross section upper limit ratios for the combined $WH/ZH/H, H \rightarrow b\bar{b}/W^+W^-/\gamma\gamma/\tau^+\tau^-$ analyses over the $100 \leq M_H \leq 200$ GeV mass range. The bands indicate the 68% and 95% probability regions where the limits can fluctuate, in the absence of signal.

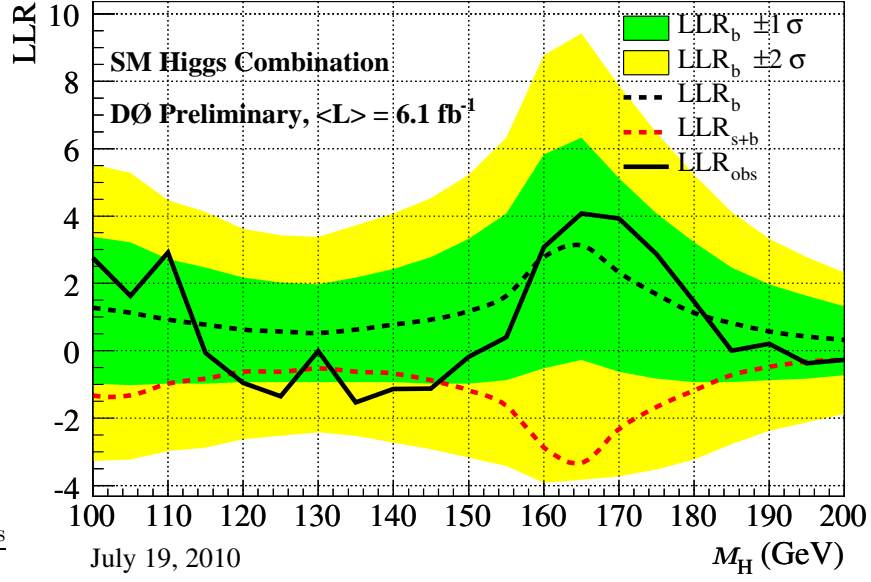


FIG. 11: Log-likelihood ratio distribution for the combined $WH/ZH/H, H \rightarrow b\bar{b}/W^+W^-/\gamma\gamma/\tau^+\tau^-$ analyses over the $100 \leq M_H \leq 200$ GeV mass range. The bands indicate the 68% and 95% probability regions for LLR_b .

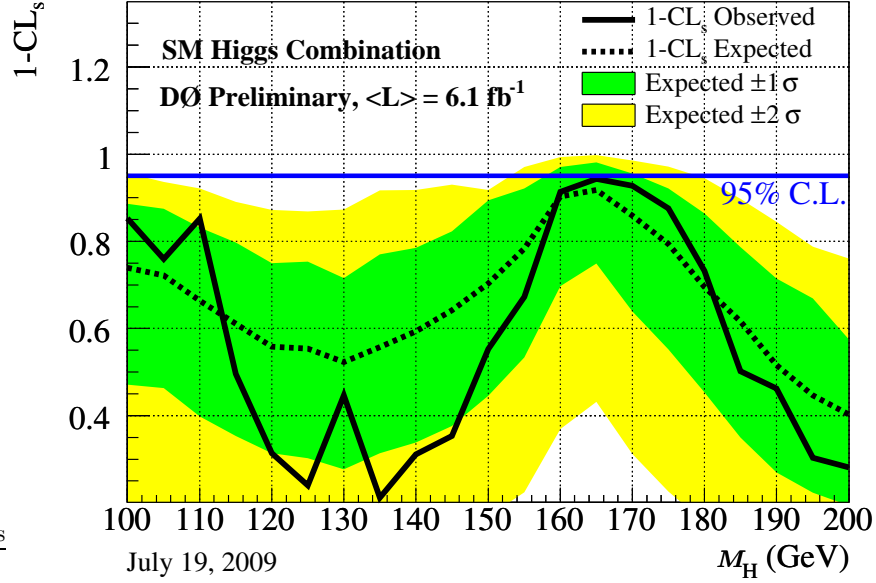


FIG. 12: The $1 - CL_S$ (exclusion probability) distribution for the combined $WH/ZH/H, H \rightarrow b\bar{b}/W^+W^-/\gamma\gamma/\tau^+\tau^-$ analyses over the $150 \leq M_H \leq 200$ GeV mass range. The bands indicate the 68% and 95% probability regions for $1 - CL_S$ Expected.

-
- [1] R. Barate *et al.* [LEP Working Group for Higgs boson searches], Phys. Lett. B **565**, 61 (2003), [arXiv:hep-ex/0306033].
 - [2] The LEP Electroweak Working Group, “Status of August 2009”, <http://lepewwg.web.cern.ch/LEPEWWG/>.
 - [3] DØ Collaboration, V. Abazov *et al.*, Nucl. Instrum. Meth. A **565**, 463 (2006) [arXiv:hep-ph/0507191].
 - [4] DØ Collaboration, DØ Note 6092-CONF.
 - [5] DØ Collaboration, DØ Note 6087-CONF.
 - [6] DØ Collaboration, DØ Note 6089-CONF.
 - [7] V.M. Abazov *et al.* (D0 Collaboration), Phys. Rev. Lett. **102**, 251801 (2009).
 - [8] DØ Collaboration, DØ Note 5845-CONF.
 - [9] DØ Collaboration, DØ Note 6082-CONF.
 - [10] DØ Collaboration, DØ Note 6006-CONF.
 - [11] DØ Collaboration, DØ Note 6095-CONF.
 - [12] DØ Collaboration, DØ Note 6091-CONF.
 - [13] DØ Collaboration, DØ Note 5858-CONF.
 - [14] DØ Collaboration, DØ Note 5739-CONF.
 - [15] T. Scanlon, FERMILAB-THESIS-2006-43.
 - [16] DØ Collaboration, DØ Note 6008-CONF.
 - [17] T. Sjöstrand, P. Edén, C. Friberg, L. Lönnblad, G. Miu, S. Mrenna and E. Norrbin, Comput. Phys. Commun. **135**, 238 (2001) [arXiv:hep-ph/0010017].
 - [18] J. Pumplin *et al.*, JHEP **0207**, 012 (2002).
 - [19] D. de Florian and M. Grazzini, Phys. Lett. B **674**, 291 (2009) [arXiv:0901.2427 [hep-ph]].
 - [20] C. Anastasiou, R. Boughezal and F. Petriello, JHEP **0904**, 003 (2009) [arXiv:0811.3458 [hep-ph]].
 - [21] A. D. Martin, W. J. Stirling, R. S. Thorne and G. Watt, Eur. Phys. J. C **63**, 189 (2009) [arXiv:0901.0002 [hep-ph]].
 - [22] J. Baglio and A. Djouadi, arXiv:1003.4266 [hep-ph].
 - [23] Private communications with J. Baglio added another decimal and extended the range to 100 GeV of [22].
 - [24] J. Campbell, K. Ellis, <http://mcfm.fnal.gov/>
 - [25] A. Djouadi, J. Kalinowski and M. Spira, Comput. Phys. Commun. **108**, 56 (1998) [arXiv:hep-ph/9704448].
 - [26] M. L. Mangano *et al.*, JHEP **0307**, 001 (2003) [arXiv:hep-ph/0206293].
 - [27] Phys. Rev. D **70**, 073011 (2004)
 - [28] A. Pukhov *et al.*, arXiv:hep-ph/9908288.
 - [29] T. Junk, Nucl. Instrum. Meth. A **434**, 435 (1999); A.Read, CERN 2000-005 (30 May 2000).
 - [30] T. Andeen *et al.*, Report No. FERMILAB-TM-2365, 2007.
 - [31] C. Anastasiou, G. Dissertori, M. Grazzini, F. Stöckli and B. R. Webber, JHEP **0908**, 099 (2009) [arXiv:0905.3529 [hep-ph]].
 - [32] W. Fisher, FERMILAB-TM-2386-E.